Tunable Dimensionality of Pinning Centers From Silver-Ion Irradiation of REBCO Coated Conductors

N. M. Strickland, A. A. Soman, N. J. Long, P. Kluth, C. Notthoff, M. W. Rupich, and S. C. Wimbush, *Senior Member, IEEE*

***Abstract*—Heavy-ion irradiation of solids produces damage tracks with radii typically of the order of 1 nm, depending on the ion species and energy. In cuprate superconductors this is close to the coherence length, which makes these defects highly effective flux pinning centers. Varying the ion-beam energy allows tuning of the dimensionality of the defects created, with higher-energy ions tending to produce columnar tracks and lower-energy ions tending to produce point-like defects. Starting with consistent production-standard REBCO tape from American Superconductor we have explored the energy-dependence of silver-ion irradiation and characterized the irradiated samples with angle-dependent transport critical current measurements. Using silver ions with energies in the range 50 MeV to 150 MeV and fluence of 4×10^{11} ions/cm^2 we have been able to tune the irradiation-induced damage from point-like defects to columnar tracks, manifesting in changes to the pinning landscape ranging from isotropic critical current enhancement to the production of strong peaks in the angle dependence of critical current.**

***Index Terms*—REBCO, ion irradiation, coated conductors, critical current anisotropy.**

I. Introduction

IRRADIATION of solid materials with high-energy ion beams is well known to produce damage tracks along the trajectory of the ions associated with collision cascades. Low-energy and low-mass ions tend to leave point-like defects whereas high-energy and high-mass ions produce continuous columnar tracks. In an intermediate regime the tracks can be columnar but discontinuous [1]. In a crystalline host material the tracks consist of highly disordered or amorphized material which makes them observable by small-angle X-ray scattering [2] or electron microscopy [3] for example.

In high-temperature superconducting (HTS) cuprate materials, ion-beam induced defects are of similar radial dimensions to the superconducting coherence length making them effective flux-pinning centers at an appropriate number density [3], [4], [5], [6], [7], [8], [9], [10], [11], [12]. Ion irradiation is therefore a useful way to study flux pinning with highly controlled variations since the defects created are nominally superposed on the existing defect landscape. The number density is easily controlled with the ion fluence and the angle of tracks by the incident angle of the ion beam. With control over track radius and length through the ion species and beam energy a range of pinning variations can be explored in a systematic way. Particularly important for such a study is the ability to probe a wide experimental parameter space of temperature, magnetic field and magnetic field angle, with populations of defects with different dimensions, aspect ratios, orientations and number density contributing to different parts of the parameter space. At high number densities defects begin to overlap thus reducing flux-pinning benefits and eventually the characteristics of a bulk superconductor will be lost.

The morphology of defects is governed largely by the electronic energy loss (also known as stopping power) $S_e = dE/dx$ of the ion beam through the target material, as this represents the linear transfer of energy to the lattice. The energy loss is a function of the ion, the target material and the ion energy and can be calculated for example through the software package SRIM [13]. Regimes of energy loss have been identified corresponding to the formation of point-like defects, overlapping point-like defects, discontinuous columnar tracks and continuous columnar tracks with threshold energy loss values of approximately 12 MeV/μm, 22 MeV/μm and 27 MeV/μm between these regimes [1].

In this study we have irradiated $REBa_2Cu_3O_7$ (REBCO) HTS coated conductors with Ag ions with energies in the range of 50 MeV to 150 MeV. Energy loss values at entry into the HTS layer range from 12 MeV/μm to 22 MeV/μm allowing us to

Manuscript received 13 November 2022; revised 12 January 2023 and 21 January 2023; accepted 22 January 2023. Date of publication 27 January 2023; date of current version 10 February 2023. This work was supported in part by the Royal Society of New Zealand under Marsden Fund Grant VUW1805. We acknowledge access to the Heavy-Ion Accelerator Facility funded under the National Collaborative Research Infrastructure Strategy (NCRIS), Australia. *(Corresponding author: N. M. Strickland.)*

N. M. Strickland, A. A. Soman, N. J. Long, and S. C. Wimbush are with the Robinson Research Institute, Victoria University of Wellington, Lower Hutt 5010, New Zealand (e-mail: nick.strickland@vuw.ac.nz; arya.ambadiyilsoman@vuw.ac.nz; nick.long@vuw.ac.nz; stuart.wimbush@vuw.ac.nz).

P. Kluth and C. Notthoff are with the Research School of Physics, Australian National University, Canberra, ACT 2601, Australia (e-mail: patrick.kluth@anu.edu.au; christian.notthoff@anu.edu.au).

M. W. Rupich is with the American Superconductor Corporation, Ayer, MA 01432 USA (e-mail: marty.rupich@amsc.com).

Color versions of one or more figures in this article are available at https://doi.org/10.1109/TASC.2023.3240384.

Digital Object Identifier 10.1109/TASC.2023.3240384

TABLE I
CALCULATED REDUCTION IN ION ENERGY DUE TO ENERGY LOSS IN THE SILVER CAP LAYER AND HTS FILM

Ion energy (MeV)			Energy loss in HTS (MeV/um)	
Incident	HTS top	HTS bottom	HTS top	HTS bottom
50	32	17	12.4	8.3
75	52	32	15.8	12.4
100	73	50	18.2	15.5
150	119	90	21.4	19.6

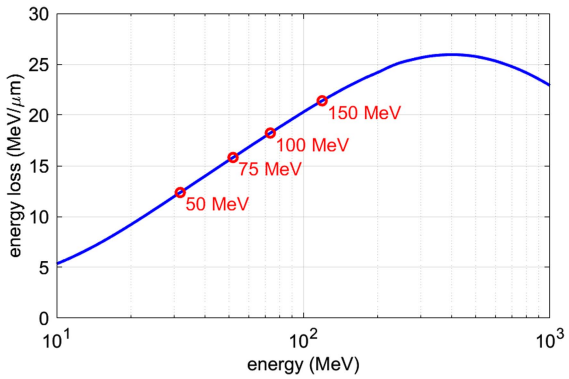

Fig. 1. Relationship between energy and electronic energy loss of high-energy Ag ions in (Y, Dy) BCO. Four points are labelled by their nominal energy at incidence to the sample, but have had their plotted energies corrected to the value at the start of the (Y, Dy) BCO film due to passage through a silver cap layer.

explore the critical current anisotropy resulting from the creation of a range of point-like to discontinuous columnar tracks.

II. EXPERIMENTAL METHODS

A. HTS Tape

The HTS samples were cut from long-length commercially available tapes from American Superconductor Corporation [14]. The nominal composition of the HTS film is $YBa_2Cu_3O_7 + 0.25\ Dy_2O_3$ with the excess rare-earth mostly forming 3D precipitates throughout the film. The Y and Dy atoms are fully intermixed between the precipitates and the REBCO matrix. The HTS film is 1.4 μm thick and is capped with a 1 μm thick silver layer, which is thinner than usual to reduce its impact on the incident ion beam. No further electroplating or lamination layers were applied. The coated conductor was annealed to a fully oxygenated state and pinning-optimized prior to the irradiation study.

A current bridge 0.5 mm wide by 5 mm long was created on each sample to reduce the area that was required to be irradiated. The bridges were created using either photolithography and wet chemical etching or a laser scriber. The critical current I_c of pristine samples was consistent across both of these methods and non-patterned samples.

B. Irradiation and Annealing

Irradiation with Ag ions was undertaken at the Heavy Ion Accelerator Facility at the Australian National University. All irradiations were conducted at normal incidence to the tape. The average ion energy decreases as the ions pass through the silver cap layer and the HTS film itself. The ion energies at the top and bottom of the HTS film have been calculated in SRIM and are summarized in Table I for the four incident energies used here. Also noted are the values of energy loss at the top and bottom of the film. Practical coated conductors often have HTS film thickness greater than 1 μm and the change in energy loss through the film can lead to different defect morphologies from top to bottom. Transport I_c then reveals an average flux pinning effect. In Fig. 1 we show the dependence of energy loss on ion energy for Ag ions within the HTS layer of our samples. The four nominal beam energies used in this work are indicated, with their energies at the top interface of the HTS layer plotted. For the remainder of this article we will label the samples with their incident beam energy.

After irradiation, the superconducting transition temperature T_c was typically degraded by several kelvin and the self-field critical current at 77 K was also degraded, as is typical following irradiation. Samples were therefore annealed in an oxygen atmosphere at 250 °C for 1 hour after irradiation to improve oxygen order in the main REBCO matrix without re-crystallizing the amorphized ion-damage tracks. The final T_c remained up to 3 K lower than the pristine starting material. Annealing improved the critical current across all temperature, field, and field angle conditions relative to the freshly irradiated samples.

C. Critical Current Measurement

Transport critical current (I_c) was measured for each sample in a SuperCurrent Measurement System [15]. The magnetic field was applied in the standard maximum Lorentz force condition, i.e., always in the plane perpendicular to the transport current. Magnetic fields of 0 T to 8 T, sample temperatures of 15 K to 90 K, and field angles of 0° to 360° could be applied. Transport currents of up to 1200 A were available, but typically less than 200 A was sufficient to reach I_c due to the narrow current bridges.

III. RESULTS AND DISCUSSION

A. Critical Current Anisotropy

The critical current anisotropy $I_c(\theta)$ at 65 K, 8 T is shown in Fig. 2 for the pristine sample and samples irradiated with Ag ions at four different energies to a fluence of 4×10^{11} ions/cm^2.

The pristine sample has quite an isotropic critical current at this condition, except for a sharp *ab*-plane peak associated with the planar stacking faults and the onset of intrinsic pinning where I_c reaches about 60% higher than the background level. Weak features emerging from a nearly isotropic background include a small *c*-axis peak and intermediate peaks at ±60°, ±120° that we will attribute to broad *c*-axis directed pinning in Section III-B below.

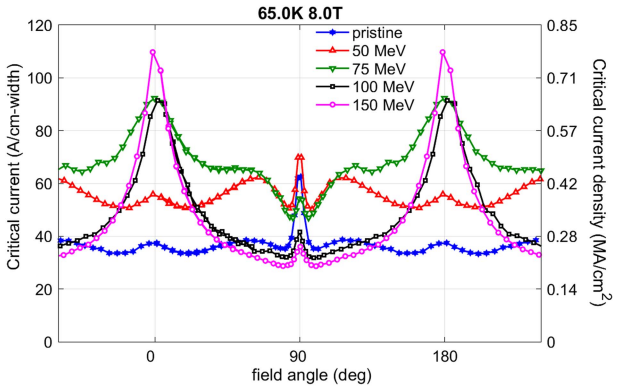

Fig. 2. Critical current anisotropy measured at 65 K, 8 T for the pristine unirradiated sample and samples irradiated at normal incidence (0°) with Ag ions at four different energies each to a fluence of 4×10^{11} ions/cm^2.

Upon irradiation with Ag ions there is a clear evolution of features with increasing beam energy. 50 MeV Ag irradiation qualitatively retains the features of the pristine sample; the main change relative to pristine being an overall lift of the isotropic background by about 50%. The small *c*-axis peak already present in the pristine sample does not increase in strength, but the intermediate peaks become slightly more pronounced. 75 MeV irradiation sees the clear emergence of a strong *c*-axis peak while also retaining the intermediate peaks. This is a clear signature of a transition from isolated point-like defects for 50 MeV to *c*-axis correlated extended discontinuous columnar tracks at 75 MeV. The *c*-axis peak further strengthens and sharpens for irradiation at higher energies of 100 MeV and 150 MeV indicating that the tracks become more and more columnar in nature, trending towards continuous columns. At 100 MeV and 150 MeV it is also notable that the intermediate peaks are significantly diminished to the point where I_c in their vicinity is lower than that of the pristine sample.

B. Maximum Entropy Model Fits

The maximum entropy vortex-path model has been shown to be a useful method for quantifying trends in angle dependences of I_c [16], [17], [18], [19], [20]. This is a conventional function-fitting approach as opposed to a field-scaling approach which cannot meaningfully describe any of the data shown in Fig. 2.

Two maximum-entropy functional forms are available, namely an angular Lorentzian:

$$I_c\ (\theta) = \frac{I_0}{\pi\,\Gamma}\ \frac{1}{\cos^2(\theta-\theta_0) + \left(1/\Gamma\right)^2 \sin^2(\theta-\theta_0)} \quad (1)$$

and an angular Gaussian:

$$I_c\ (\theta) = \frac{I_0}{\sqrt{2\pi}\,\Gamma}\ \frac{1}{\cos^2(\theta-\theta_0)} \exp\left(-\frac{\tan^2(\theta-\theta_0)}{2\Gamma^2}\right) \quad (2)$$

where in both cases Γ is a peak shape parameter (loosely, peak width), I_0 an intensity parameter and the peak is centered at $\theta = \theta_0$. Lorentzians are best restricted to $\Gamma \leq 1$ with $\Gamma = 1$ a limiting case giving a constant, fully isotropic I_c over all angles. $\Gamma > 1$ results in the same functional forms as the reciprocal values but with the peak shifted by 90° and is usually best avoided for simplicity of interpretation.

The five angle dependences of Fig. 2 are reproduced in Fig. 3(a)–(e) with fits to these functional forms. Two Lorentzians and two Gaussians are used in each case as well as an isotropic component. The two Lorentzian components fit the *ab*-plane peak at 90° (intrinsic pinning [20] or stacking faults [21]) and the *c*-axis peak at 0° which is weak in the pristine sample but becomes strong for high-energy irradiations. The ±60° and ±120° intermediate peaks can be fitted with a Gaussian centered at 0° (on the *c*-axis). A feature of the angular Gaussian lineshape is that when it becomes broad ($\Gamma > 1/\sqrt{2}$) a local minimum develops at line center and the peak bifurcates symmetrically into two peaks. This is notable since it successfully describes the intermediate peaks observed here which otherwise have no reasonable explanation in terms of inclined elongated defect structures. Instead we can interpret these peaks as arising from a broad distribution of available vortex paths with a weak c-axis bias and therefore centered at 0°. The presence of such vortex paths could be associated with grain- or twin- boundaries for example in the pristine sample and with slightly elongated defects or strings of correlated defects in irradiated samples. Such slightly elongated or correlated defects are created by 50–75 MeV Ag irradiation [22]. Fitting with a single Gaussian gives qualitatively convincing fits, however here we have used two Gaussians both centered at 0° but with Γ parameters constrained to differ by a factor of two—a pairing of lineshapes that appears to be common in conductors of this type. This use of two Gaussians yields very good and unambiguous fits and allows us to quantify the intensity and lineshape parameters of the dominant components—the two main Lorentzians—with some confidence. Selected fit parameters are plotted in Fig. 4 as a function of the incident ion energy.

Features that are clear from these fit parameters include:

- the intensity of the isotropic component associated with point-like pins increases upon irradiation at 50 MeV and 75 MeV but then decreases for 100 MeV and 150 MeV (Fig. 4(a)),
- the intensity of the *c*-axis Lorentzian associated with columnar defects is barely changed for 50 MeV but then grows (Fig. 4(a)) and sharpens (Fig. 4(b)) as the energy increases from 75 MeV, and
- the intermediate peaks fitted by *c*-axis bifurcated Gaussians associated with weakly c-axis directed pinning strengthen upon irradiation at 50 MeV and 75 MeV but then almost disappear at 100 MeV and 150 MeV (Fig. 4(c)).

All of these observations are consistent with the crossover in dimensionality from point-like defects giving nearly isotropic pinning at 50 MeV to slightly elongated defects giving both isotropic and *c*-axis enhanced pinning at 75 MeV to very elongated defects at 150 MeV giving strongly preferential *c*-axis pinning. The very broad *c*-axis directed Gaussian components are enhanced for a specific range of energies (from 50 to 75 MeV) as the new pinning centers are sufficiently short in their *c*-axis

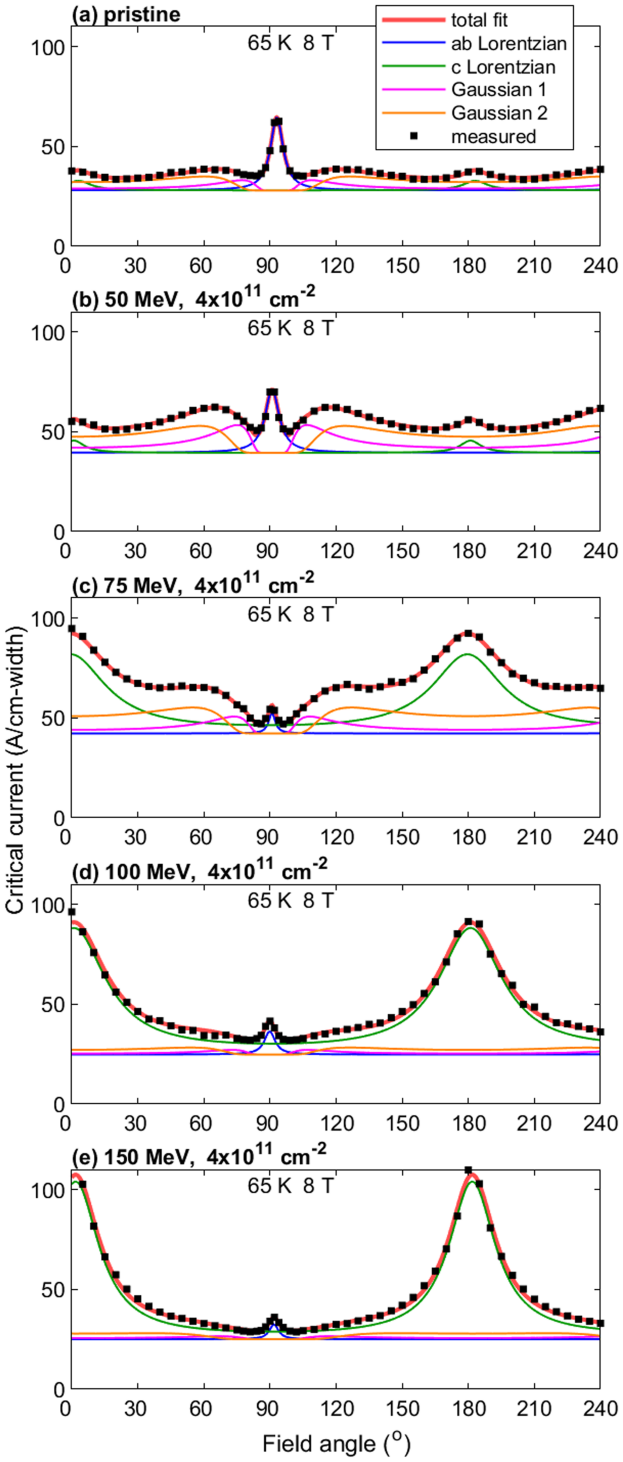

Fig. 3. Fits to the critical current anisotropy data of Fig. 2 using maximum entropy angular Lorentzian and angular Gaussian functions.

elongation to still contribute to pinning over a wide angular range. These features are then lost in favor of the sharper *c*-axis Lorentzian component as the defects become more elongated at higher energies.

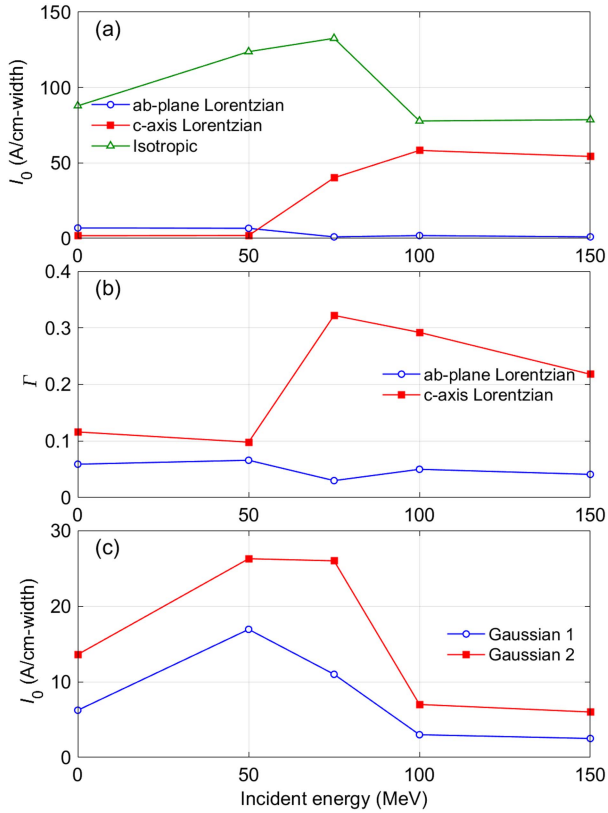

Fig. 4. Selected parameters of the maximum entropy fits of Fig. 3: (a) Intensity parameter I_0 of the isotropic and two Lorentzian components, (b) Lineshape parameter Γ of the two Lorentzian components and (c) Intensity parameter of the two broad Gaussian components.

IV. Conclusion

We have irradiated (Y,Dy)BCO coated conductors with Ag ions with incident energies ranging from 50 MeV to 150 MeV. Characterization of the critical current anisotropy shows qualitatively different outcomes over this energy range with a clear progression of additional pinning centers. 50 MeV largely increases the isotropic pinning component with no increase of the *c*-axis peak. At 75 MeV a strong *c*-axis peak appears in conjunction with the isotropic component, indicating the creation of slightly elongated ion tracks. At the higher energies, 100 MeV and 150 MeV, the *c*-axis peak grows sharper and the broad and isotropic components fall away indicating a gradual transition from point-like to elongated track defects. At the temperature and field condition examined, 65 K and 8 T, the lower ion energies of 50 MeV to 75 MeV are most effective for enhancing the angular minimum I_c whereas the higher energies promote perpendicular-field pinning at the cost of pinning at intermediate angles, especially immediately adjacent to the sharp *ab*-plane peak.

A full characterization of these effects across all temperatures and fields will open the way to using combined irradiation schemes to produce tailored pinning landscapes.

REFERENCES

[1] M. Toulemonde, S. Bouffard, and F. Studer, "Swift heavy ions in insulating and conducting oxides: Tracks and physical properties," *Nucl. Instrum. Methods B*, vol. 91, pp. 108–123, 1994.

[2] P. Kluth et al., "Fine structure in swift heavy ion tracks in amorphous SiO_2," *Phys. Rev. Lett.*, vol. 101, Oct. 2008, Art. no. 175503.

[3] L. Civale et al., "Vortex confinement by columnar defects in $YBa_2Cu_3O_7$ crystals: Enhanced pinning at high fields and temperatures," *Phys. Rev. Lett.*, vol. 67, no. 5, pp. 648–651, Jul. 1991.

[4] T. Sueyoshi, "Modification of critical current density anisotropy in high-T_c superconductors by using heavy-ion irradiations," *Quantum Beam Sci.*, vol. 5, p. 16, 2021.

[5] Y. Zhu, Z. X. Cai, R. C. Budhani, M. Suenaga, and D. O. Welch, "Structures and effects of radiation damage in cuprate superconductors irradiated with several-hundred-MeV heavy ions," *Phys. Rev. B*, vol. 48, pp. 6436–6450, 1993.

[6] N. M. Strickland et al., "Flux pinning by discontinuous columnar defects in 74 MeV Ag-irradiated $YBa_2Cu_3O_7$ coated conductors," *Physica C*, vol. 469, no. 23, pp. 2060–2067, Dec. 2009.

[7] N. M. Strickland, S. C. Wimbush, J. V. Kennedy, M. C. Ridgway, E. F. Talantsev, and N. J. Long, "Effective low-temperature flux pinning by Au ion irradiation in HTS coated conductors," *IEEE Trans. Appl. Supercond.*, vol. 25, no. 3, Jun. 2015, Art. no. 6600905.

[8] M. W. Rupich et al., "Engineered pinning landscapes for enhanced 2G coil wire," *IEEE Trans. Appl. Supercond.*, vol. 26, no. 3, Apr. 2016, Art. no. 6601904.

[9] N. M. Strickland et al., "Isotropic and anisotropic flux pinning induced by heavy-ion irradiation," *IEEE Trans. Appl. Supercond.*, vol. 32, no. 4, Jun. 2022, Art no. 8000505.

[10] M. Leroux et al., "Rapid doubling of the critical current of $YBa_2Cu_3O_{7-\delta}$ coated conductors for viable high-speed industrial processing," *Appl. Phys. Lett.*, vol. 107, 2015, Art. no. 192601.

[11] N. M. Strickland et al., *Supercond. Sci. Technol.*, 2023.

[12] K. J. Kihlstrom et al., "Large enhancement of the in-field critical current density of YBCO coated conductors due to composite pinning landscape," *Supercond. Sci. Technol.*, vol. 34, 2021, Art. no. 015011.

[13] J. F. Ziegler, M. D. Ziegler, and J. P. Biersack, "SRIM – the stopping and range of ions in matter (2010)," *Nucl. Instrum. Methods B*, vol. 268, pp. 1818–1823, Jun. 2010.

[14] M. W. Rupich et al., "Second generation wire development at AMSC," *IEEE Trans. Appl. Supercond.*, vol. 23, no. 3, Jun. 2013, Art. no. 6601205.

[15] N. M. Strickland et al., "Extended-performance SuperCurrent cryogen-free transport critical-current measurement system," *IEEE Trans. Appl. Supercond.*, vol. 31, no. 5, Aug. 2021, Art. no. 9000305.

[16] N. J. Long et al., "Relating critical currents to defect populations in superconductors," *IEEE Trans. Appl. Supercond.*, vol. 23, no. 3, Jun. 2013, Art. no. 8001705.

[17] S. C. Wimbush and N. J. Long, "The interpretation of the field angle dependence of the critical current in defect-engineered superconductors," *New J. Phys.*, vol. 14, Aug. 2012, Art. no. 083017.

[18] N. J. Long, "Model for the angular dependence of critical currents in technical superconductors," *Supercond. Sci. Technol.*, vol. 21, no. 2, Jan. 2008, Art. no. 025007.

[19] N. J. Long, "Critical current anisotropy in relation to the pinning landscape," in *Vortices and Nanostructured Superconductors*, A. Crisan, Ed., Berlin, Germany: Springer, 2008, doi: 10.1007/978-3-319-59355-5_4.

[20] N. M. Strickland, A. A. Soman, M. W. Rupich, and S. C. Wimbush, "Onset temperature of intrinsic pinning in a REBCO coated conductor from critical current anisotropy," *Superconductivity*, vol. 4, Oct. 2022, Art. no. 100025.

[21] A. A. Soman et al., "The role of stacking faults in the enhancement of the *a-b* plane peak in silver ion-irradiated commercial MOD REBCO wires," *IEEE Trans. Appl. Supercond.*, vol. 32, no. 4, Jun. 2022, Art. no. 8000405.

[22] H. Matsui and I. Yamaguchi, "Enhancement of self-field critical current density by several-tens-MeV ion irradiation in $YBa_2Cu_3O_7$ films prepared by fluorine-free metal-organic deposition," *Jpn. J. Appl. Phys.*, vol. 61, no. 4, Apr. 2022, Art. no. 043001.